RSC Advances

ROYAL SOCIETY OF CHEMISTRY

www.rsc.org/advances

RSC Advances

ARTICLE

Interband-transitions-modified third-order nonlinear optical properties of Al nanoshells in carbon disulfide†

Guangyi Jia[a] and Chungang Guo[b]

Received 00th January 20xx,
Accepted 00th January 20xx

DOI: 10.1039/x0xx00000x

www.rsc.org/

Interband transitions have important impacts on the nonlinear responses of metal nanoparticles. This work calculated the third-order nonlinear refraction index n_{2eff} and absorption coefficient β_{eff} of Al nanoshells in liquid carbon disulfide (CS_2) by using Maxwell-Garnett effective medium theory. Calculation results reveal that the interband-transitions-induced absorption (IA) of Al nanoshells can enhance the nonlinear refraction index and absorption coefficient of composite in the near-infrared region. The peak values of n_{2eff} and β_{eff} deviate from the IA peak and occur on the long-wavelength side of the interband transitions, which could be qualitatively interpreted by the increase in the linear refraction index of the CS_2 induced by the irradiation of incident light. With decreasing the nanoshell thickness, the n_{2eff} and β_{eff} peaks shift toward longer wavelengths and their deviations from the IA position become more noticeable. Besides, by controlling the nanoshell thickness together with the volume fraction of Al nanoparticles, one can optimize the nonlinear optical response of Al-CS_2 composites.

1. Introduction

Motivated by the potential applications in various optoelectronic devices, third-order nonlinear optical materials are attracting extensive interests and exploitations.[1] These materials generally have large optical nonlinearities and fast nonlinear response times, which are very suitable and versatile in data storage, optical fibers, and all-optical switching, etc.[1-4] To realize the proper nonlinear applications in devices, a variety of novel methods have been proposed to improve the nonlinear optical effects. One of these popular approaches involve the designing of metallic nanostructures which can excite strongly enhanced localized surface plasmon resonance (LSPR) fields. For example, by incorporating metal nanoparticles (NPs) on or in the expected materials, the third-order nonlinear refraction index and absorption coefficient of the nanocomposites can be increased by several or even tens of times near the LSPR wavelengths relative to those of the host matrices.[1-3,5-7] Even so, most of current researches emphasize on the use of noble metal NPs, e.g., Au, Ag, and Cu NPs, which may be due to the fact that their LSPRs generally appear in the visible region. However, noble metals are limited by resources and are very expensive. Instead, metal Al has recently been considered as a potential low-cost alternative since it supports strong LSPR from deep-ultraviolet to infrared wavelengths by well controlling nanostructures.[8-10] Especially, our recent study has shown that the LSPR of Al nanoshells can greatly enhance the third-order nonlinear optical responses of nanocomposites in the deep-ultraviolet to near-visible light region.[11]

In addition to the strong LSPR, metal Al is also an ideal material for studying the energy-band structure of simple metals since its absorption spectrum is modified by a single strong peak near 1.5 eV (~827 nm).[10] This 1.5 eV absorption peak mainly arises from the transitions between two parallel bands $\sum_3 \rightarrow \sum_1$ in the vicinity of the $\sum$ [110] axis near the K point.[10,12] The intrinsic third-order nonlinearity of metallic NPs is just closely related to the interband excitation of non-equilibrium electrons. Especially, if the pump frequency is resonant with certain interband transitions of metal, numerous electrons could be excited to the conduction bands, inducing the reduction and increase of the occupation probabilities for electron states at valence and conduction bands, respectively. As a result, the third-order nonlinearity of metal nanocomposites could be significantly modified.[13-16] Unfortunately, current studies on third-order nonlinearity near the interband transitions still mainly focus on noble metal NPs.[13-16] The impact of interband transitions of Al NPs on the third-order nonlinear effects has rarely been studied.

In this paper, we investigated the third-order Kerr-type nonlinearity of Al NPs near the interband transitions by using Maxwell-Garnett (MG) effective medium theory. Among various nanostructures, Al nanoshells are preferred here because their resonance wavelengths locate at the ultraviolet region away from the onset of interband transitions. This provides the opportunity to inspect the interband transitions alone. The surrounding medium is liquid carbon disulfide (CS_2) which is a stand reference material for characterizing third-

[a]School of Science, Tianjin University, Tianjin 300072, PR China.
[b]Key Laboratory of Beam Technology and Material Modification of the Ministry of Education, College of Nuclear Science and Technology, Beijing Normal University, Beijing 100875, PR China. E-mail: hngcg@bnu.edu.cn.

† Electronic supplementary information (ESI) available: Effects of linear refractive index of CS_2 on IA, nonlinear refraction index and absorption coefficient of an Al-CS_2 composite with t = 4 nm.

order nonlinear optical properties.[17,18] Our results show that the interband-transitions-induced absorption (IA) can enhance the third-order nonlinearity of Al-CS_2 composite in the near-infrared region. The dependence of the composite nonlinearity on the nanoshell thickness is investigated in detail. This work is useful for better understanding the nonlinear mechanism of Al nanocomposites in wavelengths where the interband transitions occur.

2. Theoretical model and linear optical properties

It is assumed that Al nanoshells are uniformly distributed in liquid CS_2. The volume fraction f of Al nanoshells is set as 0.01 unless otherwise specified. Each Al nanoshell has an outside radius R = 20 nm. In the following, we will modify and discuss the linear and nonlinear optical properties of Al-CS_2 composite by tuning the inside radius r of Al nanoshells. In order to express more clearly, Fig. 1 gives the geometry diagram of one Al nanoshell, where ε_c, ε_s, and ε_h are the dielectric constants of the core, shell, and host material, respectively. The ε_h value for CS_2 is given by $\varepsilon_h = \eta_h^2$ with η_h = 1.580826 + 15238.9/λ^2 + 4.8578×10^8/λ^4 - 8.2863×10^{13}/λ^6 + 1.4619×10^{19}/λ^8 where λ is the wavelength of incident light.[19] The ε_c value is set as 1.0, indicating a vacuum core. For the calculation of ε_s value, it is necessary to use the bulk dielectric function $\varepsilon_{bulk}(\omega)$ measured experimentally for Al, which have the contributions from interband transitions and Drude-like free electrons[20]

$$\varepsilon_{bulk}(\omega) = \varepsilon_{inter}(\omega) + \varepsilon_{free}(\omega) \quad (1)$$

In the Drude model, the free-electron dielectric function is given by

$$\varepsilon_{free}(\omega) = 1 - \frac{\omega_p^2}{\omega^2 + \Gamma_{bulk}^2} + i\frac{\omega_p^2 \Gamma_{bulk}}{\omega(\omega^2 + \Gamma_{bulk}^2)} \quad (2)$$

where ω_p is the bulk plasma frequency, ω is the optical angular frequency, and Γ_{bulk} is the bulk damping constant arising from the dispersion of electrons. For metallic nanoshells, if the shell thickness t becomes comparable or smaller than the electron mean free path l_∞ in bulk metal (l_∞ = 16 nm for Al), the scattering of free electrons on particle surface could increase the free- electron collision frequency. Therefore, the damping constant is

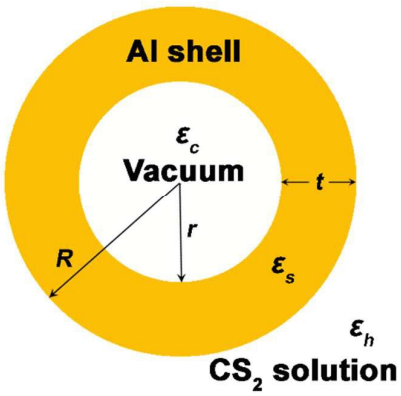

Fig. 1 Al nanoshell geometry and the defined parameters used for simulations of linear and nonlinear optical properties.

size-dependent and modified as $\Gamma = \Gamma_{bulk} + v_F/t$, where v_F is the Fermi velocity. Then the dielectric function ε_s of metallic nanoshells including both the interband tansitions part $\varepsilon_{inter}(\omega)$ and the free-electron part $\varepsilon_{free}^{NP}(\omega, t)$ can be written as

$$\begin{aligned}\varepsilon_s &= \varepsilon_{inter}(\omega) + \varepsilon_{free}^{NP}(\omega, t) \\ &= \varepsilon_{bulk}(\omega) - \varepsilon_{free}(\omega) + \varepsilon_{free}^{NP}(\omega, t) \\ &= \varepsilon_{bulk}(\omega) + \omega_p^2\left(\frac{1}{\omega^2 + \Gamma_{bulk}^2} - \frac{1}{\omega^2 + \Gamma^2}\right) \\ &\quad + i\frac{\omega_p^2}{\omega}\left(\frac{\Gamma}{\omega^2 + \Gamma^2} - \frac{\Gamma_{bulk}}{\omega^2 + \Gamma_{bulk}^2}\right)\end{aligned} \quad (3)$$

For the best fit to the dielectric function $\varepsilon_{bulk}(\omega)$ of bulk Al published by Palik,[21] the parameters of ω_p = 2.24×10^{16} rad/s, Γ_{bulk} = 7.82×10^{14} rad/s, and v_F = 1.55×10^6 m/s are utilized.

Under the condition of low-concentration Al nanoshells embedded in CS_2, MG theory considers the whole system as a homogeneous material with an effective linear dielectric function[20,22]

$$\varepsilon_{eff} = \left(\frac{1 + 2f\gamma}{1 - f\gamma}\right)\varepsilon_h,\ \gamma = \frac{\alpha}{R^3} \quad (4)$$

In the above, γ and α stand for the field enhancement factor and the quasi-static polarizability of per hollow NP, respectively. The field enhancement factor γ indicates the ratio of the internal particle response field relative to the incident field. And the quasi-static polarizability α can be described as[20,23]

$$\alpha = R^3\frac{(\varepsilon_s - \varepsilon_h)(\varepsilon_c + 2\varepsilon_s) + (r/R)^3(\varepsilon_c - \varepsilon_s)(\varepsilon_h + 2\varepsilon_s)}{(\varepsilon_s + 2\varepsilon_h)(\varepsilon_c + 2\varepsilon_s) + (r/R)^3(\varepsilon_c - \varepsilon_s)(2\varepsilon_s - 2\varepsilon_h)} \quad (5)$$

Then we can calculate the linear absorption coefficient of MG composite by

$$\sigma_{abs} = \frac{\sqrt{2}\omega}{c}\left[-\varepsilon_{eff,1} + \left(\varepsilon_{eff,1}^2 + \varepsilon_{eff,2}^2\right)^{\frac{1}{2}}\right]^{\frac{1}{2}} \quad (6)$$

where $\varepsilon_{eff,1}$ and $\varepsilon_{eff,2}$ are the real and imaginary parts of ε_{eff}, respectively, c is the velocity of light in the vacuum.

Fig. 2 shows the spectral dependence of linear absorption coefficients on nanoshell thicknesses t. In this figure as well as the following figures, "×M" (M is a number) indicates that the corresponding spectrum is obtained from multiplying the original data by M. One can see from Fig. 2 that an absorption peak originating from the LSPR of Al NPs is appeared for each t value in the short-wavelength range. As the t value decreases from 20 to 2 nm, the LSPR peak gradually shifts from 266.8 to 430.0 nm along with the widening of full width at half maximum (FWHM) and the decreasing of peak intensity. Besides the LSPR peaks in the short wavelengths, close views of the optical absorption spectra in the 700~1100 nm range (see the inset in Fig. 2) reveal that Al NPs for each t value give rise to a clear absorption band around 800~1000 nm, which can be attributed to the IA.[10] Describe in more detail, interband transitions in an

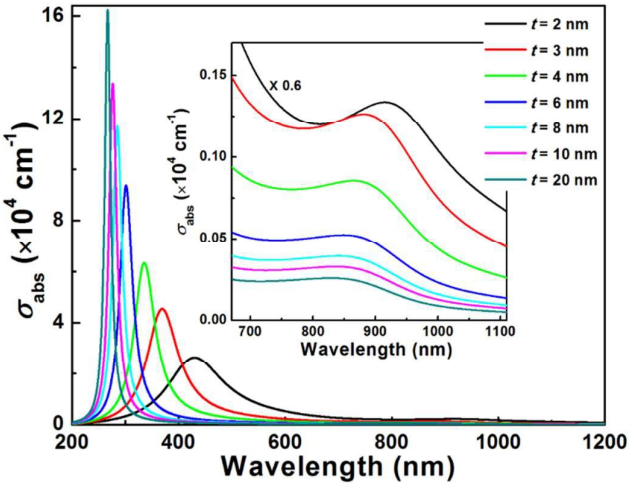

Fig. 2 Linear optical absorption coefficients of Al NPs with different nanoshell thicknesses t. The inset shows the partially magnified optical spectra for clarity.

Al NP correlate to the electron excitation from the occupied p-like states to unoccupied s-like states near the Fermi surface.[12]

On the reduction of the shell thickness, the IA peak gradually shifts toward the long-wavelength side as shown in the inserted figure in Fig. 2. According to previous studies on the IA of noble metal NPs,[24,25] the decrease of particle size could increase the discrete nature of the energy bands. This discrete nature can lead the unoccupied discrete level to shift toward the p band. As a consequence, the energy band gap could be narrowed, giving rise
to the redshift of IA.

3. Third-order nonlinear optical properties

For one third-order nonlinear optical material with a linear refractive index $\eta = n+ik$, its nonlinear complex refraction index $\eta_2 = n_2+ik_2$ is generally given by the following equations in the international system of units (SI)[26]

$$n_2 = \frac{3}{4\varepsilon_0 c\left(n^2+k^2\right)}\left[\chi_R^{(3)} + \frac{k}{n}\chi_I^{(3)}\right] \tag{7a}$$

$$k_2 = \frac{3}{4\varepsilon_0 c\left(n^2+k^2\right)}\left[\chi_I^{(3)} - \frac{k}{n}\chi_R^{(3)}\right] \tag{7b}$$

where $\chi_R^{(3)}$ and $\chi_I^{(3)}$ stand for the real and imaginary parts of the nonlinear susceptibility $\chi^{(3)}$, respectively, and $\varepsilon_0 = 8.85\times10^{-12}$ F/m is the free-space permittivity. Using Eq. (7b), we can deduce
the usually measured nonlinear absorption coefficient $\beta = 4\pi k_2/\lambda$.

According to the Z-scan measurement by using 475 fs pulses at a pumping wavelength of 1054 nm, the nonlinear refraction index n_{2h} and absorption coefficient β_h of liquid CS_2 are 0.35 nm^2/W and 8×10^{-7} nm/W, respectively.[18] In this study, values of n_{2h} and β_h are assumed to be constants in the wavelength range 650~1200 nm around the IA of Al nanoshells. Then the third-order nonlinear susceptibility $\chi_h^{(3)}$ of the liquid CS_2 can be deduced via solving the inverse expressions of Eqs. (7a-b). Accordingly, the effective nonlinear susceptibility of the composite can be calculated by[22]

$$\chi_{eff}^{(3)} = g^{(3)}\chi_h^{(3)} \tag{8}$$

with

$$g^{(3)} = \frac{1}{5}\left|\frac{\varepsilon_{eff}+2\varepsilon_h}{3\varepsilon_h}\right|^2\left(\frac{\varepsilon_{eff}+2\varepsilon_h}{3\varepsilon_h}\right)^2\left(1-f\right)\left[8f\left(1+f+f^2\right)|\gamma|^2\gamma^2 + 6f\left(1+f\right)|\gamma|^2\gamma^2 + 2f\left(1+f\right)\gamma^3 + 18f\left(|\gamma|^2+\gamma^2\right)+5\right] \tag{9}$$

Here, $g^{(3)}$ is an enhancement factor of the third-order nonlinear susceptibility, arising from the inhomogeneous distribution of the electric fields inside and outside the nanoshell. Substituting Eqs. (8-9) into Eqs. (7a-b), the nonlinear complex refraction index $\eta_{2eff} = n_{2eff} + ik_{2eff}$ of the Al-CS_2 composite can be obtained.

Fig. 3 gives the calculated nonlinear refraction index n_{2eff} (panel a) and nonlinear absorption coefficient β_{eff} (panel b). One can see from the figure that all the composites show enhanced nonlinear refraction indexes and absorption coefficients in the near-infrared region compared with the n_{2h} and β_h values of the pure liquid CS_2. Different from the previous study in which n_{2eff}

and β_{eff} could present negative values near the LSPR wavelengths,[7,11] all the values of n_{2eff} and β_{eff} are positive around the IA wavelengths. Moreover, the peak values of n_{2eff} and β_{eff} locate at the long-wavelength side of the IA, and this deviation becomes more and more noticeable as the t value decreases, as shown in Fig. 4. Around the LSPR wavelengths, the extreme value of n_{2eff} gradually shifts toward the resonance wavelength with increasing the nanoshell thickness and just appears at the LSPR position when $t = R$.[7] In contrast, the difference between the peak values of n_{2eff} (or β_{eff}) and IA tends to a nonzero constant with increasing the nanoshell thickness (see Fig. 4b). And the values of $n_{2eff,peak}$ - IA_{peak} and $\beta_{eff,peak}$ - IA_{peak} are 90.8 and 5.8 nm, respectively, for solid Al NPs with t = 20 nm.

The shell thickness-dependent electron surface scattering may account for the gradual deviations of n_{2eff} and β_{eff} peaks from the IA wavelengths with decreasing the t value.[11] Nevertheless, the n_{2eff} and β_{eff} peaks locate at the long-wavelength side of the IA wavelength even in the case of solid Al NPs, which are different from the behaviors of n_{2eff} and β_{eff} near the LSPR. This discrepancy could be qualitatively explained by the variation of the host refractive index as a high irradiance of incident light can generally increase the linear refractive index η_h of the host matrix.[7] The increase of the real part of η_h can give rise to a red-

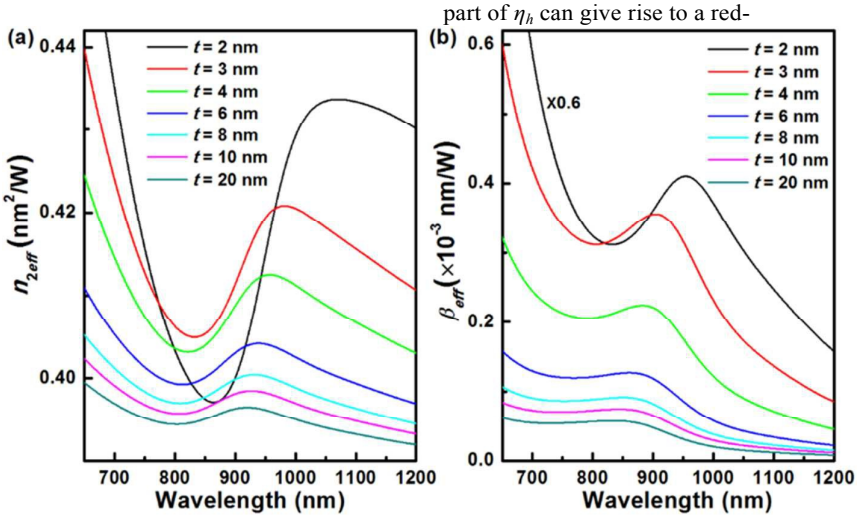

Fig. 3 Nonlinear (a) refraction indexes and (b) absorption coefficients of Al-CS_2 composites.

shift of LSPR absorption peak and the appearance of the imaginary part of η_h can broaden and weaken the resonance absorption peak of the nanocomposite.[20] However, Fig. 5a shows that the IA wavelength of solid Al NPs is nearly unchanged after an artificial increase in the real part of η_h, and the IA peak disappears after an introduction of the imaginary part in η_h. By contrast, the n_{2eff} peak gradually shifts toward long wavelengths along with the increase of k_h while its position keeps nearly unchanged after increasing n_h (Fig. 5b). As for the β_{eff} peak (Fig. 5c), it slightly shifts from 834.8 to 839.8 nm as the n_h increases to n_h+0.3, and is seriously weakened by the introduction of k_h. From these results, we can see that the increases of n_h and k_h could not induce the change of IA wavelength in solid Al NPs. Nevertheless, they could cause the redshifts of β_{eff} and n_{2eff} peaks, respectively. This could be responsible for the deviations of n_{2eff} and β_{eff} peaks from the IA wavelength in the case of solid Al NPs. By comparing Figs. 5b and c, one can also find that the redshift of n_{2eff} peak induced by increasing k_h is larger than that of β_{eff}

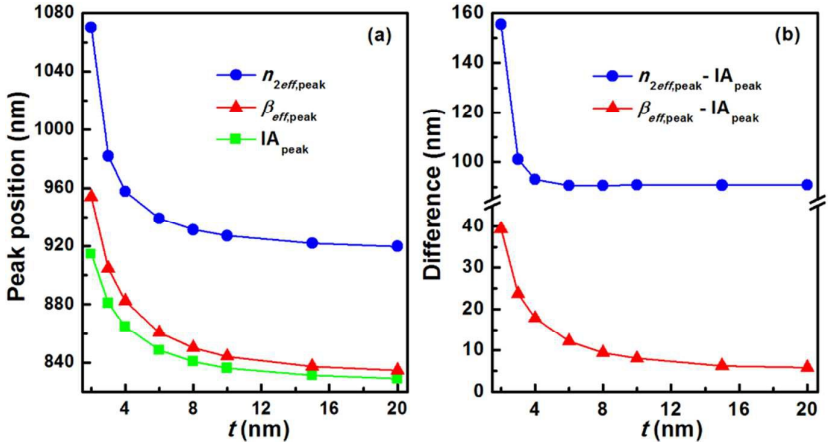

Fig. 4 (a) Peak positions of IA, n_{2eff} and β_{eff}, and (b) the differences between the peak values of n_{2eff} (or β_{eff}) and IA. Symbols are from the calculated data, and lines are just drawn as a guide to the eye.

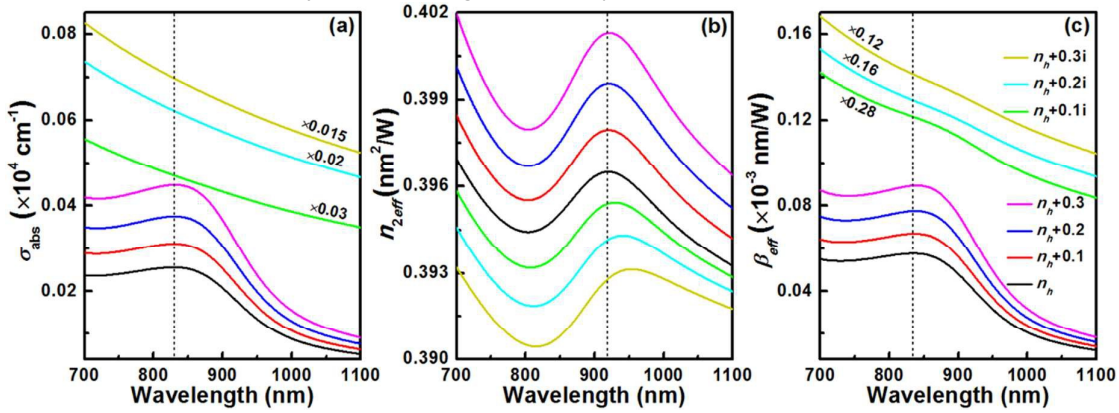

Fig. 5 (a) Linear absorption coefficient σ_{abs}, nonlinear (b) refraction index n_{2eff} and (c) absorption coefficient β_{eff} of an Al-CS_2 composite with and without artificial increases in the linear refractive index or absorption coefficient of the CS_2 host. The thickness of Al nanoshells is set as t = 20 nm. Dashed vertical lines indicate the peak positions of σ_{abs}, n_{2eff} and β_{eff} without changing the η_h value, i.e., $\eta_h = n_h$.

peak induced by increasing n_h. For hollow Al NPs, e.g., Al nanoshells with t = 4 nm as shown in Fig. S1 (see the supplementary information, ESI†), the n_{2eff} and β_{eff} peaks shift to the largest wavelengths when the k_h value increases to 0.3. However, the redshifts of n_{2eff} and β_{eff} peaks are about 43 and 35 nm, respectively. These results mean that the largest redshift of n_{2eff} peak induced by changing the host refractive index is larger than that of β_{eff} peak. This may explain why the n_{2eff} peaks are longer than β_{eff} peaks as shown in Fig. 3 and why the $n_{2eff,peak}$ - IA$_{peak}$ values are much larger than $\beta_{eff,peak}$ - IA$_{peak}$ values as shown in Fig 4b.

To evaluate the interplay between the linear and nonlinear absorptions near the interband transitions, the transmitted intensity I_{out} being a function of irradiance intensity I_{inc} is calculated at 850 nm. Considering the presence of both linear and third-order nonlinear absorptions in the media, one can obtain the transmitted intensity by[27]

$$I_{out} = \frac{I_{inc}(1-R)^2\exp(-\sigma_{abs}L)}{1+(\beta_{eff}/\sigma_{abs})I_{inc}(1-R)[1-\exp(-\sigma_{abs}L)]} \quad (10)$$

where L is the length of the sample, and

$$R = \left(\frac{n_{eff}-1}{n_{eff}+1}\right)^2 \quad (11)$$

is the reflectivity at normal incidence, and n_{eff} is the real part of linear refractive index of the composite.

Fig. 6a presents the intensity transmitted through one Al-CS_2 composite with L = 10 μm. One can see from the figure that the transmission function is nearly linear at lower irradiance intensities. As the value of I_{inc} increases, the nonlinear effect becomes noticeable and I_{out} begins to deviate from the linear response. An irradiance threshold value at which I_{out} deviates from the linear transmission by 50 percent can be defined. And this irradiance threshold value decreases from ~1.9×10^5

GW/cm^2 for t = 20 nm to ~5.2×10^4 GW/cm^2 for t = 2 nm. Further increasing the irradiance intensity will lead the total transmitted intensity to become saturated. Because the nonlinear absorption coefficient β_{eff} increases as the nanoshell becomes thinner as shown in Fig. 3b, the saturation intensity transmitted through the sample decreases with reducing the t value. Besides, the linear transmission in the lower irradiance intensities also decreases with reducing the t value. This could originate from the interband-transitions-induced linear absorption that gradually increases with decreasing the nanoshell thickness as observed in the inset in Fig. 2. These results mean that one challenge being similar with that occurs in utilizing LSPR to enhance the nonlinear refraction and absorption may also exist in the current case: even if the nonlinear response can be enhanced by the IA,

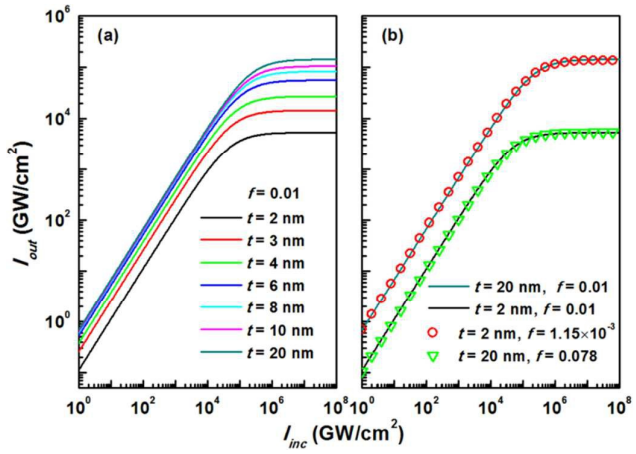

Fig. 6 Transmitted intensity as a function of irradiance intensity at 850 nm for Al-CS_2 composites with different nanoshell thicknesses t and volume fractions f.

the linear loss induced by interband transitions should be minimized.

Apart from the nanoshell thickness t, the volume fraction f of NPs is also one important factor to modify the transmission function.[7] The larger volume fraction generally gives a larger linear absorption coefficient. Nevertheless, the thicker Al nanoshells present a lower linear absorption value near the IA wavelength as shown in the inset in Fig. 2. Considering this, it is possible to obtain the similar transmission function curves by simultaneously increasing the nanoshell thickness and the volume fraction of Al NPs. For example, the I_{out} values of Al-CS_2 composite with t = 2 nm and f = 0.01 are close to those of composite with t = 20 nm and f = 0.078 as shown in Fig. 6b. Additionally, Fig. 6b also shows that if the nanoshell is fixed, one can enhance the nonlinear transmitted intensity by decreasing the volume fraction. Combining the nanoshell thickness with the volume fraction provides more degrees to modulate and optimize the nonlinear response of metallic nanocomposites.

4. Conclusions

On the basis of MG theory, we investigated the influence of interband transitions on the third-order nonlinear optical properties of Al nanoshells in liquid CS_2. Our results reveal that the IA can enhance the nonlinear optical response of Al-CS_2 composite in the near-infrared region. It may be due to the increase in the linear refraction index of the host matrix induced by the irradiation of incident light, the n_{2eff} and β_{eff} peaks appear at the long-wavelength side of the IA wavelength for the solid Al NPs, which are distinct from the behaviors of n_{2eff} and β_{eff} near the LSPR. As the nanoshell becomes thinner, the n_{2eff} and β_{eff} peaks shift toward longer wavelengths and their deviations from the IA wavelength become more noticeable. For a fixed volume fraction of Al NPs, the nonlinear transmitted intensity decreases with reducing the nanoshell thickness. If the nanoshell thickness keeps unchanged, one can obtain the enhanced nonlinear transmitted intensity by decreasing the volume fraction of NPs. These results may provide insights into the interplay between the interband transitions and the third-order nonlinearity of Al NPs, and give more degrees to modify and optimize the nonlinear optical properties of nanocomposites.

Notes and references

1. A. L. Stepanov, *Rev. Adv. Mater. Sci.*, 2011, **27**, 115–145.
2. O. Sánchez-Dena, P. Mota-Santiago, L. Tamayo-Rivera, E. V. García-Ramírez1, A. Crespo-Sosa, A. Oliver and J.-A. Reyes-Esqueda, *Opt. Mater. Express*, 2014, **4**, 92–100.
3. W. D. Xiang, H. H. Gao, L. Ma, X. Ma, Y. Y. Huang, L. Pei and X. J. Liang, *ACS Appl. Mater. Interfaces*, 2015, **7**, 10162−10168.
4. C. L. Wu, Y. H. Lin, S. P. Su, B. J. Huang, C. T. Tsai, H. Y. Wang, Y. C. Chi, C. I. Wu and G. R. Lin, *ACS Photonics*, 2015, **2**, 1141−1154.
5. C. Zheng, W. Z. Chen, Y. Y. Huang, X. Q. Xiao and X. Y. Ye, *RSC Adv.*, 2014, **4**, 39697–39703.
6. G. Y. Jia, H. T. Dai, X. Y. Mu, C. G. Guo and C. L. Liu, *Opt. Mater. Express*, 2015, **5**, 1156–1167.
7. D. C. Kohlgraf-Owens1 and P. G. Kik, *Opt. Express*, 2008, **16**, 16823–16834.
8. M. Honda, Y. Kumamoto, A. Taguchi, Y. Saito and S. Kawata, *Appl. Phys. Lett.*, 2014, **104**, 061108.
9. O. Lecarme, Q. Sun, K. Ueno and H. Misawa, *ACS Photonics*, 2014, **1**, 538−546.
10. C. Langhammer, M. Schwind, B. Kasemo and I. Zorić, *Nano Lett.*, 2008, **8**, 1461−1471.
11. G. Y. Jia, C. L. Liu and H. T. Dai, *Plasmonics*, 2015, **10**, 211–217.
12. H. Ehrenreich, H. R. Philipp and B. Segall, *Phys. Rev.*, 1963, **132**, 1918−1928.
13. M. Kauranen and A. V. Zayats, *Nat. Photonics*, 2012, **6**, 737−748.
14. M. Conforti and G. D. Valle, *Phys. Rev. B*, 2012, **85**, 245423.
15. L. Yang, D. H. Osborne, R. F. Haglund Jr., R. H. Magruder, C.W. White, R. A. Zuhr and H. Hosono, *Appl. Phys. A*, 1996, **62**, 403−415.

16. A. Marini, M. Conforti, G. Della Valle, H. W. Lee, Tr. X. Tran, W. Chang, M. A. Schmidt, S. Longhi, P. St. J. Russell and F. Biancalana, *New J. Phys.*, 2013, **15**, 013033.
17. M. Reichert, H. Hu, M. R. Ferdinandus, M. Seidel, P. Zhao, T. R. Ensley, D. Peceli, J. M. Reed, D. A. Fishman, S. Webster, D. J. Hagan and E. W. Van Stryland, *Optica*, 2014, **1**, 436–445.
18. R. A. Ganeev, *J. Opt. A: Pure Appl. Opt.*, 2005, **7**, 717–733.
19. A. Samoc, J. Appl. Phys., 2003, 94, 6167–6174.
20. U. Kreibig and M. Vollmer, *Optical properties of metal clusters*, 1995, Springer, Berlin.
21. E. D. Palik, *Handbook of optical constants of solids*, 1985, New York.
22. M. I. Stockman, K. B. Kurlayev and T. F. George, *Phys. Rev. B* 1999, **60**,17071–17083.
23. M. Moskovits, I. Srnová-Šloufová and B. Vlčková, *J. Chem. Phys.*, 2002, **116**,10435–10446.
24. B. Balamurugan and T. Maruyama, *Appl. Phys. Lett.*, 2005, **87**, 143105.
25. B. Balamurugan and T Maruyama, *J. Appl. Phys.*, 2007, **102**, 034306.
26. R. del Coso and J. Solis, *J. Opt. Soc. Am. B*, 2004, **21**, 640–644.
27. P. Liu, W. L. Smith, H. Lotem, J. H. Bechtel, N. Bloembergen and R. S. Adhav, *Phys. Rev. B*, 1978, **17**, 4620–4632.